Ion kinetic dynamics in strongly-shocked plasmas relevant to ICF

2017 Nucl. Fusion 57 066014

(http://iopscience.iop.org/0029-5515/57/6/066014)

IOP Publishing | International Atomic Energy Agency Nuclear Fusion

Nucl. Fusion **57** (2017) 066014 (6pp) https://doi.org/10.1088/1741-4326/aa69d9

Ion kinetic dynamics in strongly-shocked plasmas relevant to ICF

H.G. Rinderknecht[1], P.A. Amendt[1], M.J. Rosenberg[2], C.K. Li[3], J.A. Frenje[3], M. Gatu Johnson[3], H. Sio[3], F.H. Séguin[3], R.D. Petrasso[3], A.B. Zylstra[4], G. Kagan[4], N.M. Hoffman[4], D. Svyatsky[4], S.C. Wilks[1], V. Yu. Glebov[2], C. Stoeckl[2] and T.C. Sangster[2]

[1] Lawrence Livermore National Laboratory, Livermore, CA 94550, United States of America
[2] Laboratory for Laser Energetics, University of Rochester, Rochester, NY 14623, United States of America
[3] Plasma Science and Fusion Center, Massachusetts Institute of Technology, Cambridge, MA 02139, United States of America
[4] Los Alamos National Laboratory, Los Alamos, NM 87545, United States of America

E-mail: rinderknecht1@llnl.gov

Received 16 December 2016, revised 1 March 2017
Accepted for publication 29 March 2017
Published 20 April 2017

Abstract

Implosions of thin-shell capsules produce strongly-shocked ($M > 10$), low-density ($\rho \sim 1$ mg cc^{-1}), high-temperature ($T_i \sim$ keV) plasmas, comparable to those produced in the strongly-shocked DT-vapor in inertial confinement fusion (ICF) experiments. A series of thin-glass targets filled with mixtures of deuterium and Helium-3 gas ranging from 7% to 100% deuterium was imploded to investigate the impact of multi-species ion kinetic mechanisms in ICF-relevant plasmas over a wide range of Knudsen numbers ($N_K \equiv \lambda_{ii}/R$). Slightly kinetic implosions ($N_K \sim 0.01$–0.05) follow the expected yield trend with experimentally-inferred N_K, suggesting effects associated with long mean-free-paths (such as energetic tail-ion loss) provide the dominant yield reduction mechanisms. In contrast, highly kinetic implosions (Rinderknecht et al 2015 *Phys. Rev. Lett.* **114** 025001) with inferred $N_K > 0.5$ produce the opposite yield trend from the Knudsen-number prediction, confirming the dominance of multi-species physics in these experiments. The impact of the observed kinetic physics mechanisms on the formation of the hotspot in ICF experiments is discussed.

Keywords: inertial confinement fusion, kinetic plasmas, multi-species plasmas, laser fusion experiments

(Some figures may appear in colour only in the online journal)

1. Introduction

Understanding the evolution of the plasma during the shock transit phase is fundamentally important for achieving ICF hotspot ignition, because the shock sets the initial conditions for hotspot formation, compression, ignition and burn [1]. In the NIC point design for ignition on the NIF, four shocks compress the cryogenic deuterium-tritium (DT) fuel, then combine into a single strong shock with Mach number ~10–50 [2]. This strong shock transits the central gas, a DT-vapor with initial density 0.3 mg cc^{-1}, compressing it by a constant factor but heating the plasma proportionally to M^2. This produces the conditions for long ion–ion mean-free-paths, which scale as $\lambda_{ii} \propto (T^2/n) \propto M^4$. Quantitatively, calculations of the ion–ion mean-free-paths in the shocked central plasma based on hydrodynamic simulations predict that they reach $\lambda_{ii} \approx 100$ μm, comparable to the scale size of the implosion [3]. Such conditions are precisely those in which the hydrodynamic assumptions begin to break down and kinetic physics becomes important.

ICF experiments are generally designed using radiation-hydrodynamic simulations of a single ion-species plasma. Recent implosions varying the density of the fuel demonstrated that such simulations increasingly overpredict the fusion yield

and burn-averaged ion temperature as the ion–ion mean-free-path in the fuel during burn increases [3, 4]. Defining the Knudsen number as the ratio between the average ion–ion mean-free-path and the hot-spot radius during peak nuclear production, $N_K = \langle\lambda_{ii}\rangle/R$, for implosions with $N_K > 0.1$ the nuclear yield was reduced relative to the hydrodynamic predictions by a factor of $\sim 0.1/N_K$. This effect was reasonably explained by the direct reduction of the fusion reactivity by the loss of the energetic tail ions which dominate fusion [5–7], and the dilution and loss of fuel from the core due to ion diffusion into the shell plasma during the implosion [4, 8].

Recent experimental [9–13] and theoretical work [14–18] has also investigated the impact of multiple ion species on ICF implosions. Deuterium-^{3}He gas-filled implosions that produce conditions relevant to the shock phase of ICF have demonstrated that simulations increasingly overpredict the nuclear yield as the fraction of ^{3}He in the fuel is increased [13]. For high-density implosions with moderate Knudsen numbers ($N_K \lesssim 1$), diffusive separation of the ion species was found to be dominant. Low-density implosions ($N_K \sim 10$) demonstrated evidence of thermal decoupling between the two ion species.

The effects of long mean-free-paths and multiple ion species have so far been studied separately. However, because the mean-free-path for a given ion depends upon the charge and mass of all species in the plasma, the effects of long mean-free-paths will couple to ion concentration. The mean-free-path for an ion of species j interacting with species k is given by the formula:

$$\lambda_{j,k} = \frac{3}{4\pi}\left(\frac{4\pi\epsilon_0}{e^2 Z_j Z_k}\right)^2 \frac{T^2 m_j}{n_k m_r \ln\Lambda}, \qquad (1)$$

where $Z_{j,k}$ are the ionization states, $m_{j,k}$ the ion masses- and m_r the reduced mass, T the ion temperature of both species, n_k the field ion density, and $\ln\Lambda$ the Coulomb logarithm. When multiple species are present, the total mean-free-path for species j is the inverse sum of the mean-free-path relative to all species: $\lambda_j = \left[\sum_k \lambda_{j,k}^{-1}\right]^{-1}$. Assuming thermalized ion species and ignoring variations in the Coulomb logarithm, the scaling of the mean-free-path for ions in a D-^{3}He plasma with constant mass density ρ can be calculated as a function of the deuterium fraction, $f_D \equiv n_D/(n_D + n_{^3He})$:

$$\lambda_D = \frac{10(3-f_D)}{(24-19f_D)}\lambda_C, \qquad \lambda_{^3He} = \frac{5(3-f_D)}{8(5-4f_D)}\lambda_C, \qquad (2)$$

where the constant of proportionality $\lambda_C = (3/4\pi)(4\pi\epsilon_0/e^2)^2 T^2 m_p/(\rho \log\Lambda)$. The deuteron mean-free-path λ_D is always $3.3 \times \lambda_{^3He}$ to within 5%; additionally, the mean-free-path for each species increases by greater than $3\times$ as f_D increases from 0 to 1. This reduced confinement with increasing f_D stems primarily from the decrease in average field ion charge, partially offset by an increase in the ion number density with constant ρ ($\lambda_{ii} \propto \langle m\rangle/\langle Z\rangle^2$). An average mean-free-path for the plasma, calculated by weighting the species-specific λ_i by their concentrations, is more than $10\times$ greater for pure deuterium than for pure ^{3}He. Because of this strong dependence of N_K on f_D, experimental studies must be careful to distinguish between observed trends due to the 'single-species' effects of large N_K and the multi-species effects dependent on f_D.

Data from D^{3}He-gas filled implosions with low and high Knudsen numbers and varying deuterium fraction illuminate the interaction of the two previously studied classes of kinetic phenomena—long mean-free-path effects and multi-species effects—and demonstrate that different physics dominates the observed nuclear performance trends in the low- and high-N_K regimes. In this paper, section 2 describes the design of experiments to probe kinetic fuel dynamics as a function of Knudsen number and fuel concentration. The results are presented in section 3 and discussed in section 4. Finally, the relevance of these results to ICF hotspot formation is discussed in section 5.

2. Experimental design

The experiments were performed in two campaigns at the 60-beam OMEGA laser [19]. In the first campaign, spherical glass capsules (860 μm diameter, 2.2 μm wall) were filled with various concentrations of D_2 and ^{3}He gas. The deuterium fraction of the gas fills ranged from $f_D = 1$ (pure deuterium) to 0.07 (^{3}He-rich), while maintaining a constant initial mass density of $\rho_0 = 0.4, 1.5,$ or 3.3 mg cc^{-1}. The capsules were imploded by direct laser drive, using a 23 TW pulse with duration of 0.6 ns (low, high density) or 1.0 ns (mid density). These implosions produced hot ($\langle T_i\rangle \sim 10$–$20$ keV), low density plasmas, generating moderately to extremely kinetic conditions with Knudsen numbers in the range $N_K \sim 0.1 - 20$.

In the second campaign, gold hohlraums (1.6 mm diameter, 2 mm long, with 0.8 mm diameter laser entrance holes) were used to indirectly drive thin glass shell targets filled with either pure deuterium or 50:50 D:^{3}He gas. The capsules had an outer diameter of 625 μm, 5.1 μm walls, and a fill gas density of 6.1 mg cc^{-1}. Forty beams containing 17.6 kJ in a 1 ns impulse drove the hohlraums. Due to the reduced efficiency of indirect drive and the increased gas density, these implosions produced cooler ($\langle T_i\rangle \sim 2$–$6$ keV), denser plasmas with Knudsen numbers on the order of $N_K \sim 0.01$.

In both series of experiments, the shells burn through prior to shock rebound and the compression of the fuel by remaining shell mass is minimal. For this reason the experiments probe the shock-phase dynamics of plasmas relevant to the central DT-plasma at the beginning of the deceleration phase in laser-driven ICF designs. Such 'exploding pusher' experiments have been demonstrated to be insensitive to departures from 1D physics, because of low radial convergence, reduced hydrodynamic instability growth, and the insensitivity of spherically converging shocks to drive asymmetry [20, 21]. The 1D nature of these implosions makes them especially valuable for the study of deviations from hydrodynamics in imploded plasmas, because the multi-dimensional hydrodynamic effects that can dominate high-convergence implosions (e.g. instability growth, turbulent mix) are minimized. Moreover, D^{3}He fuels with constant mass density

Table 1. Experimental nuclear yields, burn-averaged temperatures, and inferred Knudsen numbers (averaged over # shots).

Density mg cc^{-1}	f_D	# shots	Yields DD-n	Yields D^3He-p	$\langle T_i \rangle_{DDn}$ keV	$\langle N_K \rangle$
6.08	1	3	$(4.9 \pm 0.4) \times 10^{-8}$		2.6 ± 0.4	0.046 ± 0.015
(Indirect)	0.5	3	$(1.7 \pm 0.2) \times 10^{-8}$	$(6.8 \pm 0.4) \times 10^{-6}$	2.9 ± 0.9	0.016 ± 0.008
3.29	1	2	$(2.1 \pm 0.2) \times 10^{-11}$		10.8 ± 0.4	
	0.8	1	$(1.2 \pm 0.1) \times 10^{-11}$	$(2.6 \pm 0.3) \times 10^{-10}$	10.9 ± 0.5	1.16 ± 0.19
	0.5	2	$(2.3 \pm 0.2) \times 10^{-10}$	$(3.0 \pm 0.2) \times 10^{-10}$	11.9 ± 0.6	0.69 ± 0.11
1.45	1	3	$(1.7 \pm 0.2) \times 10^{-11}$		12.0 ± 0.6	1.30 ± 0.67
	0.46	3	$(1.8 \pm 0.2) \times 10^{-10}$	$(3.8 \pm 0.6) \times 10^{-10}$	13.3 ± 0.6	0.42 ± 0.12
	0.07	4	$(3.5 \pm 0.5) \times 10^{-8}$	$(8.7 \pm 0.8) \times 10^{-9}$	14.2 ± 2.3	0.22 ± 0.08
0.39	1	3	$(3.2 \pm 0.6) \times 10^{-10}$		18.6 ± 0.4	18.5 ± 3.8
	0.8	1	$(2.0 \pm 0.2) \times 10^{-10}$	$(2.5 \pm 0.2) \times 10^{-10}$	18.5 ± 0.5	9.4 ± 1.4
	0.5	2	$(5.1 \pm 0.3) \times 10^{-9}$	$(2.5 \pm 0.2) \times 10^{-10}$	17.6 ± 1.7	5.1 ± 2.2
	0.2	2	$(7.0 \pm 1.1) \times 10^{-8}$	$(1.2 \pm 0.2) \times 10^{-10}$	19.3 ± 2.1	4.1 ± 0.6

are hydrodynamically equivalent, such that within each shot series, systematic perturbations to the hydrodynamic evolution should affect all shots equally, and should not introduce trends that depend on deuterium fraction [9]. By comparing the results of experiments in which N_K ranges from 0.01–20 and f_D from 0.07–1.0, the relative importance and impact of mean-free-path scale effects (such as the Knudsen tail ion loss) and multi-species effects (such as ion species separation and thermal decoupling) are studied.

3. Experimental results

Comprehensive nuclear diagnosis was performed to study the fuel dynamics in these implosions. Yields and spectra of DD-fusion neutrons (2.45 MeV) and D^3He-fusion protons (14.7 MeV) were measured using the neutron time-of-flight (nTOF) diagnostic suite [22] and the Wedge–Range–Filter proton spectrometers (WRF), respectively; protons were measured with the charged particle spectrometers (CPS1 and CPS2) for the direct-drive implosions only [23]. Burn-averaged ion temperatures $\langle T_i \rangle$ were inferred from the spectral widths of the nuclear products [24]. For the low- and high-density direct-drive implosions, the spatial burn profiles of D^3He-protons and DD-protons (3.0 MeV) were measured by penumbral imaging [25]. The shell trajectory was recorded using time-resolved self-emission x-ray imaging [26]. The measured yields and ion temperatures are shown in table 1.[5] 1D-radiation hydrodynamic simulations of the direct-drive implosions were performed using the code HYADES [27] for comparison. The indirect-drive implosions were also simulated using a radiation-hydrodynamic code. Simulations were constrained using experimentally observed bang-times, laser coupling, and hohlraum radiation.

The reduction in yield relative to 1D as a function of fuel density in similar shock-driven experiments has been described previously [3, 4]; to study the trends with deuterium fraction

[5] The yield and $\langle T_i \rangle$ data from the low- and high-density direct-drive implosions were first reported in [13].

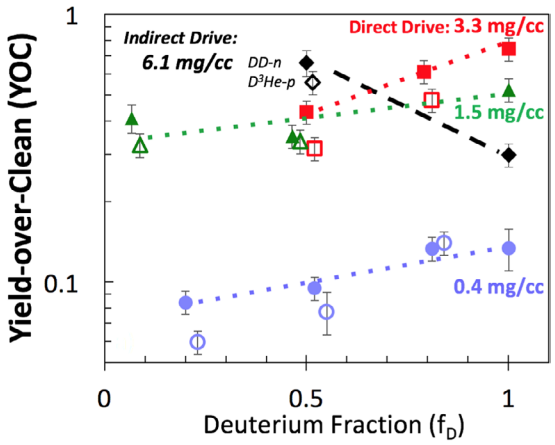

Figure 1. Measured nuclear yields divided by simulated yield ('Yield-over-clean') for direct-drive implosions with fuel density 3.3 (■), 1.5 (▲), and 0.4 mg cc^{-1} (●), and for indirect-drive implosions with fuel density 6.1 mg cc^{-1} (◆). Solid symbols indicate DD-neutrons; open symbols indicate D^3He-protons. Dashed lines are included to guide the eye.

it is convenient to examine the ratio of measured to simulated yields ('Yield-over-clean' or YOC), as shown in figure 1. The direct- and indirect-drive campaigns exhibit clear, opposite trends in YOC with f_D: while the direct-drive implosion performance is reduced with smaller f_D, the indirect-drive implosion performance is reduced with greater f_D. The contrasting trends suggest different physical effects dominate the loss of performance in the two regimes.

The dominant difference between these campaigns is the collisionality of the fuel, which is quantified by the Knudsen number. A 'burn-averaged Knudsen number' $\langle N_K \rangle \equiv \langle \lambda_{ii} \rangle / R_{burn} \propto \langle T_i \rangle^2 / \langle n_i \rangle R_{burn}$ may be calculated using the measured burn-average temperatures, radius at peak emission R_{burn}, and the inferred fuel density during burn $\langle n_i \rangle$. For eight low- and two high-density direct-drive implosions, a burn-average ion density was calculated from the measured nuclear yield, temperature, burn-history and burn volume data, as described in [13]. On the mid-density direct-drive

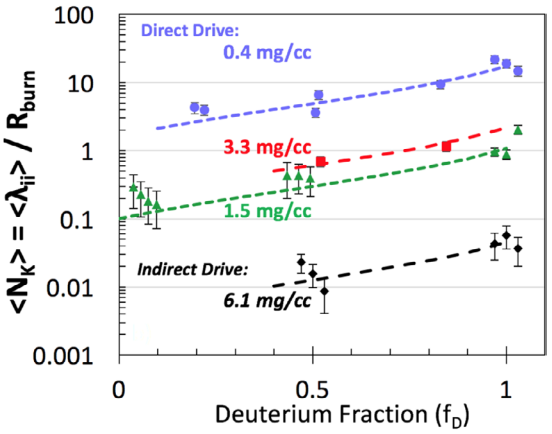

Figure 2. Inferred burn-averaged Knudsen numbers for direct-drive implosions with fuel density 3.3 (■), 1.5 (▲), and 0.4 mg cc^{-1} (●), and for indirect-drive implosions with fuel density 6.1 mg cc^{-1} (◆); points spread out for clarity. Knudsen numbers increase with deuterium fraction in agreement with theory (dashed lines; absolute value fit to data). The indirect-drive implosions are substantially more hydrodynamic than direct-drive due to reduced energy coupling to the fuel.

campaign, since penumbral images were not recorded, the density of the $f_D = 1$ implosions was calculated using the inferred areal density at burn ρR_{burn} from the secondary D-T and D-^{3}He fusion yield [28], assuming that density scales with convergence cubed. For the remainder of the mid-density shots, the density was calculated assuming the same average convergence as for the deuterium shots. On the indirect-drive campaign, the radius at bang-time $R_{burn} \sim 230$ μm was inferred from self-emission x-ray radiographs, and the density was calculated from the initial density $n_{i,0}$ using the scaling relation: $\langle n_i \rangle = n_{i,0}(R_{burn}/R_0)^3$. These values were used to calculate $\langle N_K \rangle$, as shown in figure 2; average quantities are listed in table 1. The theoretical trend of $\langle N_K \rangle$ with f_D is calculated using equation 2 and fits are included in figure 2; the predicted trends match well the trends in the experimental data.

4. Discussion

Based on Knudsen-layer theory and the scaling observed in [4], pure deuterium implosions would be expected to underperform compared to the D^{3}He-filled implosions: equation 2 predicts the deuterium Knudsen number to increase by a factor of 2.32× from $f_D = 0.5$ to $f_D = 1$, or from $N_K \sim 1.9\%$ to $\sim 4.5\%$ based on the values inferred from data. This predicted trend is observed in the indirect-drive implosions.

To estimate the impact of Knudsen tail ion loss on the yields in these experiments, the spherical geometry must be taken into account. The values of $\langle N_K \rangle$ shown in figure 2 are calculated for the center of the plasma, but the local Knudsen number (and associated reactivity reduction) in general depends only on distance to the nearest boundary. The spherical solution has been obtained by solving numerically the constrained PDE problem formulated by the quasi-stationary kinetic equation along with the constraint that no suprathermal ion inflow exists from the cold plasma into the hot-spot [7]. For the experimental plasma conditions, the volume-averaged reactivity was calculated to be reduced to 89% of the Maxwellian reactivity for the 50:50 D:^{3}He case, and 78% for the pure deuterium. This calculation follows the observed and expected trend with f_D, and accounts for approximately one third of the reduction observed in the data (YOC of 65% and 30%, respectively). A scaling offset in YOC may be caused by incorrect coupling of energy to the implosion in the simulations. However, due to the hydrodynamic equivalence of D^{3}He fuels with equal mass density, a change in coupling should not introduce a trend with deuterium fraction [9]. The remaining trend may be associated with the diffusive loss of bulk fuel ions and contamination of the fuel, which similarly increases with N_K; the diffusive loss of deuterons from the fuel was found to be the largest factor in yield reduction for moderately kinetic experiments ($N_K \sim 0.2$) [4]. Note that the reactivity reduction with increased f_D is accentuated by the changing composition of the background plasma, which affects the shape of the modified distribution functions.

In contrast, the opposite trend is observed in the direct-drive data, for which the implosions with $f_D = 1$ perform better than D^{3}He mixtures. In previous work, these trends have been successfully explained by diffusive separation of the fuel ion species for the high-density case, and thermal decoupling of the ion species in the low-density case [13]. Those explanations stand, however it is important to consider why they dominate over the long mean-free-path mechanisms in the high-N_K experiments. The reactivity reduction formalism is perturbative in the suprathermal ions, and strictly valid only in the regime $N_K \ll 1$. When mean free paths become comparable to the size of the fuel, fusion is no longer dominated by thermal processes, but rather by the density and velocity of the radially-streaming bulk ion populations. As such, the Knudsen number loses relevance as a metric for fusion reactivity. Instead, processes that modify the plasma conditions prior to burn dominate the fusion output. These include ion species separation, which concentrates ^{3}He relative to D in the fuel during the implosion phase; and thermal decoupling of the D and ^{3}He in the shock, which alters the energy balance between these two species. Both of these multi-species effects reduce the performance of mixtures relative to pure fuels, as shown in the data.

5. Conclusion

Nuclear data from D^{3}He-gas filled implosions with varying Knudsen number and deuterium fraction demonstrate a change in the regime of dominant kinetic physics impacting the nuclear performance. Knudsen-layer tail-ion-loss dominates for low Knudsen numbers ($N_K \sim 0.01$), while multi-species effects dominate for high Knudsen numbers ($N_K \gtrsim 0.5$). This suggests that at intermediate Knudsen-numbers ($N_K \sim 0.1$) the effects of long mean-free-paths and of multi-species effects on the yield trend are balanced. Indeed, the mid-density experiments may bridge this transition: as shown in figure 1, both the ^{3}He-rich implosions ($N_K \approx 0.2$) and the pure-D implosions ($N_K \approx 1.3$) perform similarly or better than the

$f_D = 0.5$ implosions ($N_K \approx 0.4$), suggesting a combination of the tail-ion-loss and multi-species trends. A more thorough exploration of N_K versus f_D space would be valuable to identify this transition point.

In D-T, the primary fuel of interest for fusion ignition, the mean-free-paths of the two species are more comparable: λ_D is smaller than λ_T by a factor of ~0.8. Because of this, the average $\langle \lambda_{ii} \rangle$ and Knudsen number decrease with increased f_D when maintaining mass density in DT plasmas. This trend is opposite of the trend in D^3He; as such, long mean-free-path effects and multi-species effects will both tend to reduce performance of DT mixtures relative to pure deuterium. However, because of the reduced magnitude of the N_K dependence on f_D (~1/3 × as compared to ~10×), deuterium-tritium mixtures better decouple the effects of long mean-free-paths from multi-species dynamics, making DT valuable for future ion kinetic physics studies.

The plasmas studied in this work are relevant to the shocked DT-vapor at the onset of deceleration in ICF experiments, for which $N_K \sim 0.2$–0.8 [3]. While the nuclear yield at this phase of the experiment is negligible, the state of the central plasma is important in establishing the trajectory of deceleration for the cold fuel. Standard hydrodynamic methods assume the shocked vapor is isentropically compressed and heated by the ice layer; heat flow from the core then ablates material from the inside of the cryogenic fuel, which forms the bulk of the hot spot mass. However the present work suggests that the core ions are already far from Maxwellian: $N_K = 0.5$ implies ~7/8 of the core volume is within one mean-free-path of the wall. In this scenario, hydrodynamic estimates of compressional heating and heat transport will not apply. Instead, free-streaming particles will rapidly deposit their kinetic energy in the cold fuel, or gain energy by reflection without significantly reducing fuel velocity. These processes will continue until energy loss from the core or increased density from continuing compression and mass ablation reduce the mean-free-paths, and hydrodynamics regains validity. This kinetic volume will change the initial conditions for the subsequent fuel assembly and hotspot formation.

The creation of this kinetic volume seems to be a general feature of laser-driven hotspot ignition designs, for which the low central vapor density $\rho = 0.3$ mg cc^{-1} is set by the vapor pressure of the cryogenic DT fuel layer, and rapid implosion of the solid fuel leads to strongly-shocked vapor. Alternative laser-driven designs, such as fast ignition [29] or shock ignition [30], could circumvent this kinetic behavior, since the compression of the fuel is less extreme and is not relied on for hotspot formation. MagLIF implosions [31] also do not include strong shocks and rely on magnetic fields rather than collisions to confine the hotspot plasma.

Kinetic physics has been shown to impact hotspot formation and nuclear performance of multi-species plasmas in simulations relevant to ICF [17, 32], and may contribute to the observed low areal densities and high ion temperatures of layered DT experiments at the NIF when compared to hydrodynamic predictions. Experimentally, this hypothesis can be tested by varying the Knudsen number of the initial DT vapor, which can be done using liquid DT layers [33]. Improved understanding of the kinetic dynamics of hotspot formation through Vlasov–Fokker–Planck or hybrid-PIC simulations will inform and support the continued use of hydrodynamic tools to design an igniting ICF implosion. This work performed under the auspices of the U.S. Department of Energy by LLNL under Contract DE-AC52-07NA27344 and supported in part by the National Laser User's Facility (Grant No. DE-NA0002035).

References

[1] Goldstein W.H. 2012 *Science of Fusion Ignition on NIF* LLNL-TR-570412, Lawrence Livermore National Laboratory (https://doi.org/10.2172/1061032)

[2] Haan S.W. *et al* 2011 Point design targets, specifications, and requirements for the 2010 ignition campaign on the National Ignition Facility *Phys. Plasmas* **18** 051001

[3] Rosenberg M.J. *et al* 2014 Investigation of ion kinetic effects in direct-drive exploding-pusher implosions at the NIF *Phys. Plasmas* **21** 122712

[4] Rosenberg M.J. *et al* 2014 Exploration of the transition from the hydrodynamiclike to the strongly kinetic regime in shock-driven implosions *Phys. Rev. Lett.* **112** 185001

[5] Molvig K. *et al* 2012 Knudsen layer reduction of fusion reactivity *Phys. Rev. Lett.* **109** 095001

[6] Albright B.J. *et al* 2013 Revised Knudsen-layer reduction of fusion reactivity *Phys. Plasmas* **20** 122705

[7] Kagan G. *et al* 2015 Self-similar structure and experimental signatures of suprathermal ion distribution in inertial confinement fusion implosions *Phys. Rev. Lett.* **115** 105002

[8] Hoffman N.M. *et al* 2015 Approximate models for the ion-kinetic regime in inertial-confinement-fusion capsule implosions *Phys. Plasmas* **22** 052707

[9] Rygg J.R. *et al* 2006 Tests of the hydrodynamic equivalence of direct-drive implosions with different D_2 and ^3He mixtures *Phys. Plasmas* **13** 052702

[10] Wilson D.C. *et al* 2008 The effects of pre-mix on burn in ICF capsules *J. Phys.: Conf. Ser.* **112** 022015

[11] Herrmann H.W. *et al* 2009 Anomalous yield reduction in direct-drive deuterium/tritium implosions due to ^3He addition *Phys. Plasmas* **16** 056312

[12] Casey D.T. *et al* 2012 Evidence for stratification of deuterium-tritium fuel in inertial confinement fusion implosions *Phys. Rev. Lett.* **108** 075002

[13] Rinderknecht H.G. *et al* 2015 Ion thermal decoupling and species separation in shock-driven implosions *Phys. Rev. Lett.* **114** 025001

[14] Amendt P. *et al* 2010 Plasma barodiffusion in inertial-confinement-fusion implosions: application to observed yield anomalies in thermonuclear fuel mixtures *Phys. Rev. Lett.* **105** 115005

[15] Kagan G. *et al* 2014 Thermo-diffusion in inertially confined plasmas *Phys. Lett.* A **378** 1531

[16] Bellei C. *et al* 2014 Species separation and kinetic effects in collisional plasma shocks *Phys. Plasmas* **21** 056310

[17] Inglebert A. *et al* 2014 Species separation and modification of neutron diagnostics in inertial-confinement fusion *Europhys. Lett.* **107** 65003

[18] Kagan G. *et al* 2016 Influence of coupling on thermal forces and dynamic friction in plasmas with multiple ion species (arXiv:1609.00742)

[19] Boehly T.R. *et al* 1997 Initial performance results of the OMEGA laser system *Opt. Commun.* **133** 495

[20] Rinderknecht H.G. *et al* 2014 First observations of nonhydrodynamic mix at the fuel-shell interface in shock-driven inertial confinement implosions *Phys. Rev. Lett.* **112** 135001

[21] Rygg J.R. *et al* 2008 Observations of the collapse of asymmetrically driven convergent shocks *Phys. Plasmas* **15** 034505
[22] Glebov V.Y. *et al* 2004 Prototypes of National Ignition Facility neutron time-of-flight detectors tested on OMEGA *Rev. Sci. Instrum.* **75** 3559
[23] Séguin F.H. *et al* 2003 Spectrometry of charged particles from inertial-confinement-fusion plasmas *Rev. Sci. Instrum.* **74** 975
[24] Ballabio L. *et al* 1998 Relativistic calculation of fusion product spectra for thermonuclear plasmas *Nucl. Fusion* **38** 1723
[25] Séguin F.H. *et al* 2006 Measured dependence of nuclear burn region size on implosion parameters in inertial confinement fusion experiments *Phys. Plasmas* **13** 082704
[26] Bradley D.K. *et al* 1995 Development and characterization of a pair of 30–40 ps x-ray framing cameras *Rev. Sci. Instrum.* **66** 716
[27] Larsen J.T. *et al* 1994 HYADES—A plasma hydrodynamics code for dense plasma studies *J. Quantum Spectrosc. Radiat. Transfer* **51** 179
[28] Cable M.D. *et al* 1987 Neutron spectra from inertial confinement fusion targets for measurement of fuel areal density and charged particle stopping powers *J. Appl. Phys.* **62** 2233
[29] Tabak M. *et al* 1994 Ignition and high gain with ultrapowerful lasers *Phys. Plasmas* **1** 1626
[30] Betti R. *et al* 2007 Shock ignition of thermonuclear fuel with high areal density *Phys. Rev. Lett.* **98** 155001
[31] Slutz S.A. and Vesey R.A. 2012 High-gain magnetized inertial fusion *Phys. Rev. Lett.* **108** 025003
[32] Peigney B.E. *et al* 2014 Ion kinetic effects on the ignition and burn of inertial confinement fusion targets: a multi-scale approach *Phys. Plasmas* **21** 122709
[33] Olson R.E. *et al* 2013 Alternative hot spot formation techniques using liquid deuterium-tritium layer inertial confinement fusion capsules *Phys. Plasmas* **20** 092705